Fatigue failure behavior of Super304H welded joint at elevated temperatures

Geun Dong Song [a,*], Jeong Ho Hwang [b], Seung Heon Baek [a], Hee Kwon Ku [a], Dong Seok Lim [a], Beom Kyu Kim [a]
[a] Institute of Future Energy Technology, FNC Technology Co., Ltd, 44, Tapsil-ro, Giheung-gu, Yongin-si, Gyeonggi-do, Korea, 16954
[b] Material and Component Convergence Center, Korea Construction Equipment Technology Institute, 52, Saemangeumsandan 2-ro, Gunsan-si, Jeollabuk-do, Republic of Korea, 54002,
**Corresponding author: gdsong@fnctech.com*

1. Introduction

Super304H is attracting great attention as a promising candidate material for heat exchanger tube at ultra-supercritical conditions, due to its desirable combination of superior thermal conductivity, corrosion and oxidation resistance, and creep properties [1].

Heat exchanger tubes are used in various complex shapes to meet design requirements and improve thermal efficiency, and hence, the welding of Super304H tubes to other components is imperative. It is known that welded parts are the most vulnerable sections, causing a significant deterioration of strength, ductility, and creep and corrosion resistance [2]. In this regard, the mechanical properties of the Super304H welded joint, in particular its fatigue properties, are a key factor in ensuring the structural reliability [3]. Despite its importance, however, the mechanical properties, including the tensile and fatigue properties of the Super304H base metal (BM) and its welded joint have rarely been reported.

In this work, we explored the microstructural evolution of BM and weld metal (WM) of Super304H welded joints during fatigue deformation at 600 ◦C and their effect on the local mechanical properties of both weld regions. We combined microstructural analyses using optical microscopy (OM), scanning electron microscopy (SEM), energy-dispersive X-ray spectroscopy (EDS), and X-ray diffraction (XRD) with local hardness measurements using nanoindentation. The detailed fatigue failure mechanisms were explained based on the relationship between the local hardness inhomogeneity and strain localization in the welded joint.

2. Experimental procedures

2.1 Material and microstructure characterization

The base and filler metal used in this work were Super304H tubes with an outer diameter of 42.2 mm and thickness of 6.6 mm and T-304H rods with a diameter of 2.4 mm, respectively. Their chemical composition is given in Table. 1.

The Super304H tubes were cut into smaller tubes of lengths 50 mm and 70 mm and then welded using a total of five passes of direct current straight polarity manual gas tungsten arc welding with a 60° V-shaped groove and 3 mm root gap. The detailed welding process is given elsewhere [4].

To characterize the microstructural features of the welded joint, cuboidal specimens with dimensions of 26 mm × 6 mm × 2 mm, including BM, heat-affected zone (HAZ), and WM, were machined from the Super304H welded tubes. This specimen was embedded in a cold mounting resin, polished with diamond pastes. Next, the surfaces of the specimens were electrochemically etched at an applied voltage of 6 V for 20 s in 2 wt% oxalic acid solution. After the etching process, the specimen surfaces were observed and analyzed using OM, SEM, EDS, and XRD.

Table 1. Chemical composition of base and filler metal.

Material	Element (wt%)											
	C	Si	Mn	P	S	Ni	Cr	Mo	Cu	Nb	N	Fe
Base metal	0.09	0.21	0.76	0.06	0.01	8.39	17.8	-	2.87	0.42	0.2	Bal.
Filler metal	0.13	0.3	3.2	0.03	0.03	16.0	18.0	0.9	3.0	0.6	0.15	Bal.

2.2 Hardness test

Vickers hardness tests were conducted on the cross-section of the welded joints, including BM, HAZ, and WM, with the same specimens used for microstructural characterization. Indentations were made with a load of 500 gf for 10 s, and the distance between the indentations was kept at 0.3 mm to exclude the effect from nearby indentations. Nanoindentation tests were also conducted on BM and WM of the welded joint to measure the local hardness. Indentation arrays (4 × 10) were set on BM and WM to make indentations to 200 nm depth, while a distance of 20 μm was kept between indentations to exclude the effect from nearby indentations. After the nanoindentation tests, the indentation locations were carefully examined to determine the correlation between the microstructure and local hardness.

2.3 Low-cycle fatigue test

Low-cycle fatigue test specimens were machined from Super304H welded tubes as shown in Fig. 1. The machined specimen included with BM, HAZ, and WM, where the WM was placed at the center of the gauge section.

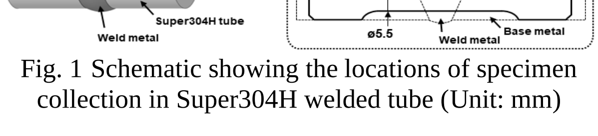

Fig. 1 Schematic showing the locations of specimen collection in Super304H welded tube (Unit: mm)

The gauge sections were 16 mm in length and 6 mm in diameter for the fatigue test specimen. Fatigue tests were conducted using a hydraulic material testing machine with 100 kN capacity. For accurate measurement and control of strain during the test, a high-temperature uniaxial extensometer with a gauge length of 12 mm was used. Low-cycle fatigue tests were conducted under a fully reversed strain control mode with a triangular waveform at 600 °C. The strain rate was fixed at 5×10^{-3} s^{-1} and total strain amplitudes of 0.25 to 1.0 % were used.

3. Results and discussion

3.1. Fatigue resistance

The total strain amplitude-fatigue life data of the welded joint at 600 °C are presented in Fig. 2(a), and the data of BM are inserted for comparison. The welded joint shows a general tendency of metallic materials, i.e., the fatigue life decreases with increasing strain amplitude. The fatigue resistance of the welded joint is comparable to that of BM at high strain amplitudes of ≥ ~0.4%, but there is a drastic reduction in the fatigue resistance of the welded joint as compared to that of BM as the strain amplitude reduces to less than 0.4%. This is associated with the shift of the fatigue failure location from BM at high strain amplitudes of ≥ ~0.4% (Fig. 2(b)) to WM at low strain amplitudes of < ~0.4% (Fig. 2(c)).

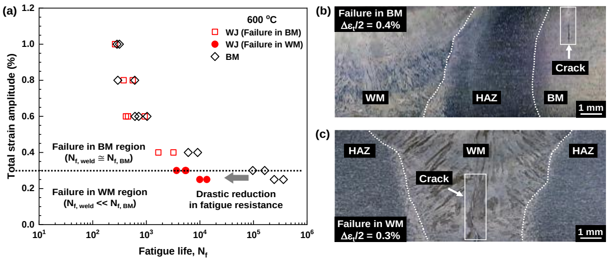

Fig. 2. Low-cycle fatigue life behavior of the Super304H welded joint at 600 °C: (a) $\Delta\varepsilon_t$-N_f curve and optical micrographs showing the longitudinal section of the specimens fatigue-failed at (b) $\Delta\varepsilon_t/2$=0.4% and (c) $\Delta\varepsilon_t/2$=0.3%.

3.2. Microstructure and local mechanical property

To examine the microstructural evolutions in BM and WM of the welded joint during the fatigue test, we conducted thermal aging experiments at 600 °C for aging times of 2 and 8 h; the two thermal aging times were determined considering that the time required for inducing fatigue failure location shift at 600 °C was less than ~5 h but more than ~3 h.

The microstructure of WM in the welded joint and its evolution during thermal aging are shown in Fig. 3. For the as-welded material, rod-like precipitates observed in the interdendritic regions (IDR) were identified as Nb (C, N) phase by EDS analysis, as shown in Fig. 3(a). After thermal aging for 2 h, no change was observed in the dendrite core (DC) and the Nb (C, N) phase (Fig. 3(b)). However, small precipitates were formed in IDR, away from the Nb (C, N) phase. As the thermal aging time increased to 8 h (Fig. 3(c)), the number and size of precipitates formed in IDR increased significantly, whereas DC and Nb (C, N) phase remained unchanged.

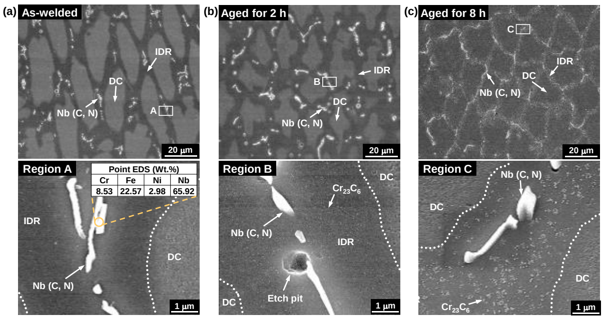

Fig. 3. Microstructural evolution in WM of the welded joint during thermal aging at 600 °C. (a) As-welded material, (b) aged for 2 h, and (c) aged for 8 h.

Fig. 4 presents the nanoindentation hardness of the three important microstructural features, i.e., the grain interior of BM, and DC and IDR of the WM, and their evolution with increasing thermal aging time.

The three microstructural features exhibit a distinct difference in the variation of hardness with thermal aging time. In WM, there was no change in the hardness of DC on thermal aging, as it retained the initial hardness of 3.07 GPa, whereas the hardness in IDR increased significantly from 3.36 GPa (as-welded material) to 3.77 GPa (material aged for 8 h). As for the grain interior of BM, the hardness markedly increases from 2.68 GPa (as-welded material) to 3.36 GPa (material aged for 8 h) with thermal aging, even though there is no change in the microstructure. It is known that the secondary Nb (C, N) phase, which is nanometer-sized and beyond the spatial resolution of the SEM used in this work, precipitates in the grain interior of Super304H steel during thermal aging at 625 and 650 °C [6] and induces a hardening effect.

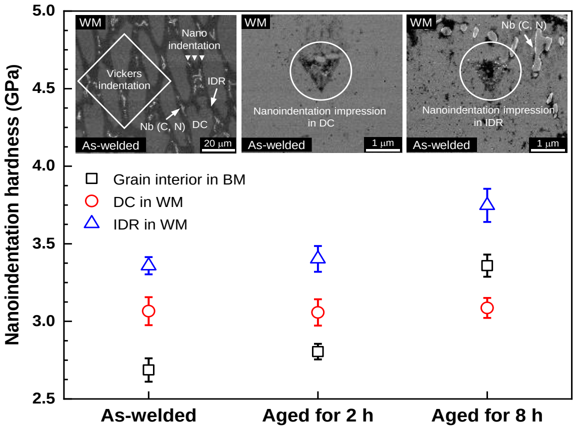

Fig. 4. Change in nanoindentation hardness between DC and IDR in WM and grain interior in BM with thermal aging time.

3.3. Ftigue failure mechanisms

Fig. 5 presents the optical and SEM micrographs of the longitudinal sections of the specimens that fatigue-failed at 600 °C. At a high strain amplitude of 0.4%, fatigue failure occurred in BM (Fig. 5(a) and (b)). A main crack initiated on the specimen surface and propagated to the interior along the direction perpendicular to the loading axis in the transgranular mode. At a low strain amplitude of 0.3%, the fatigue failure location shifts to WM (Fig. 5(c)). The magnified SEM image of region B in Fig. 5(c) shows the precipitation of $Cr_{23}C_6$ carbides in IDR and absence of any microstructural change in DC, which is identical to the microstructures developed in the material aged for 8 h (Fig. 5(d)). Different microstructural evolutions occur in each region of the welded joint, promoting inhomogeneity of local hardness and thereby altering the softest region to DC in WM. Fig. 5(e) and (f) show the magnified SEM images of the crack initiation region C and crack tip region D in Fig. 5(c). It is evident that a main crack initiates in DC on the specimen surface and propagates to the interior along DC.

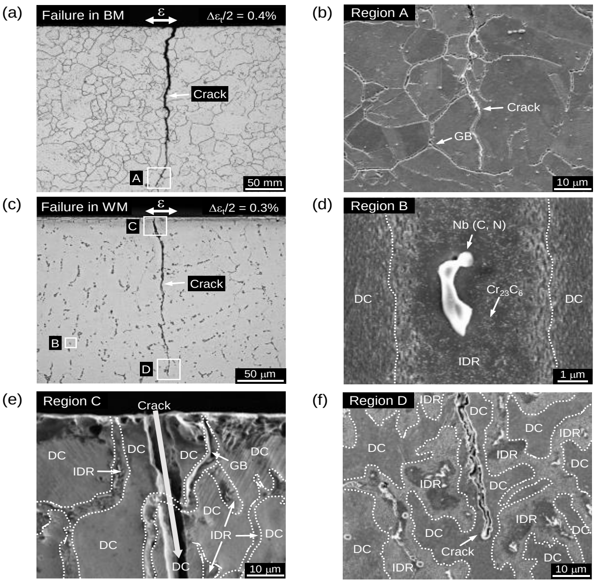

Fig. 5. Optical and SEM micrographs showing the two different fatigue failure mechanisms of the welded joint at 600 °C. (a) The fatigue-failed specimen at $\Delta\varepsilon_t/2$ = 0.4% and (b) magnified SEM image of region A in (a). (c) The fatigue-failed specimen at $\Delta\varepsilon_t/2$ = 0.3% and magnified SEM images of regions (d) B, (e) C, and (f) D in (c).

4. Conclusion

The effect of thermal aging on the microstructure and fatigue properties of Super304H welded joint was investigated. A thermal aging effect promotes different microstructural evolutions in BM and WM, deepening material inhomogeneity in the welded joint, and thereby triggering strain localization in WM. The intensified local hardness inhomogeneity caused the softest zone at the welded joint, wherein strain localization occurred, serving as a crack nucleation site and propagation path, to shift from BM to WM. Consequently, the thermal aging effect induced a shift in the failure location from BM to WM.

Acknowledgements

This work was supported by the National Research Foundation of Korea (NRF) grant funded by the Korea government (2022M2D4A1054827).

REFERENCES

[1] X.M. Li, Y. Zou, Z.W. Zhang, and Z.D. Zou, Microstructure evolution of a novel Super304H steel aged at high temperatures, Materials Transaction, 51, pp. 305–309. 2010.

[2] W. Liu, F. Lu, Y. Wei, Y. Ding, P. Wang, and X. Tang, Special zone in multi-pass welded metal and its role in the creep behavior of 9Cr-1Mo welded joint, Materials and Design, 108, pp. 195–206, 2016.

[3] J.H. Lee, J.H. Hwang, and D.H. Bae, Welding residual stress analysis and fatigue strength assessment at elevated temperature for multi-pass dissimilar material weld between alloy 617 and P92 steel, Metals and Materials International, 24, pp. 877–885, 2018.

[4] J. H. Hwang, G. D. Song, D. Kim, Y. Huh, B. C. Park, J. Hahn, and S. G. Hong, Tensile and fatigue properties of Super304H welded joint at elevated temperatures, Interntional Journal of Fatigue, 143, 105989, 2021.

[5] X. Wang, Y. Li, D. Chen, J. Sun, Precipitate evolution during the aging of Super304H steel and its influence on impact toughness, Materials Science and Engieering A, 685, pp. 238–245, 2019.